# Size-selective synthesis of calix[*n*]furan[2*n*]thiazoles bearing *meso*-$CH_2$ bridges

**Kotaro Shibata[a], Takuma Nakabayashi[a], Keita Watanabe[a], Yuki Ide[b], Tomoya Ichino[*b], and Yasuhide Inokuma[*a,b]**

[a]*Division of Applied Chemistry, Faculty of Engineering, Hokkaido University, Kita 13 Nishi 8 Kita-ku, Sapporo, Hokkaido 060-8628, Japan*

[b]*Institute for Chemical Reaction Design and Discovery (WPI-ICReDD), Hokkaido University, Kita 21, Nishi 10, Kita-ku, Sapporo, Hokkaido, 001-0021, Japan.*

*Received date (to be automatically inserted after your manuscript is submitted)*

*Accepted date (to be automatically inserted after your manuscript is accepted)*

**ABSTRACT:** Size-selective synthesis of calixpyrrole-related macrocycles remains challenging, particularly for ring-contracted and expanded analogues, although calix[4]-type macrocycles are often obtained as major products via conventional acid-catalyzed condensation reactions of aryl monomers. Here, we found that strain-based design of thiazole-containing macrocycles enables size-selective synthesis of calix[*n*]furan[2*n*]thiazoles (*n* = 1 or 2) in which two thiazole units are linked by a methylene bridge. The DFT calculation through StrainViz analysis revealed that calix[1]furan[2]thiazole bearing a methylene bridge had a total strain of 11.2 kcal/mol, which was smaller than that of calix[3]pyrrole (13.4 kcal/mol). The target calix[1]furan[2]thiazole was almost exclusively formed in 45% yield by a Hantzsch reaction between the corresponding bis(α-bromoketone) and bis(thioamide) at 0.50 mM concentration. When the substrate concentration was increased above 10 mM, the calix[6]-type product, calix[2]furan[4]thiazole, was formed as the major product. Despite the existence of the *meso*-$CH_2$-bridge, the obtained macrocycles were stable to air-oxidation. Acid-catalyzed hydrolysis of the furan rings in calix[1]furan[2]thiazole and subsequent Paal–Knorr reaction afforded calix[1]pyrrole[2]thiazole. We also found that the deformation angles α determined from the single crystal X-ray structures show a good correlation with the total strain and synthetic yield of calix[3]-type compounds via direct macrocyclization.

**KEYWORDS:** macrocycle, calixpyrrole, strained macrocycle, Hantzsch reaction, Paal–Knorr reaction

*Correspondence to: Tomoya Ichino, Institute for Chemical Reaction Design and Discovery (WPI-ICReDD), Hokkaido University, Kita 21, Nishi 10, Kita-ku, Sapporo, Hokkaido, 001-0021, Japan TEL: +81-(0)11-706-9668, e-mail: tichino@eis.hokudai.ac.jp; Yasuhide Inokuma, Division of Applied Chemistry, Faculty of Engineering, Hokkaido University, Kita 13 Nishi 8 Kita-ku, Sapporo, Hokkaido 060-8628, Japan TEL: +81-(0)11-706-6556, FAX: +81-(0)11-706-6557, e-mail: inokuma@eng.hokudai.ac.jp.

## INTRODUCTION

Calix[*n*]pyrroles and their related macrocycles, consisting of various heteroarenes such as thiophene, furan, and pyridine, have attracted much attention in the light of anion binding [1], metal complexation [2], chemo-sensor [3], and so forth. The size of these macrocycles, defined as the number of heteroarenes *n*, is a crucial factor for binding specific guest molecules and ions in a selective fashion. However, conventional acid-catalyzed pyrrole condensation reactions typically afford calix[4]pyrroles as the major product [4], rendering the synthesis of ring-contracted [5] and expanded [6] analogues ($n = 3$ and $n \geq 5$, respectively) rather laborious. In addition, the incorporation of other heteroarenes, such as thiophene, imidazole, and pyridine, into calix-type macrocycles is also a typical issue in this research area, because the reactivity of these arenes toward electrophiles in the aromatic electrophilic substitution differs significantly from that of pyrrole [7,8].

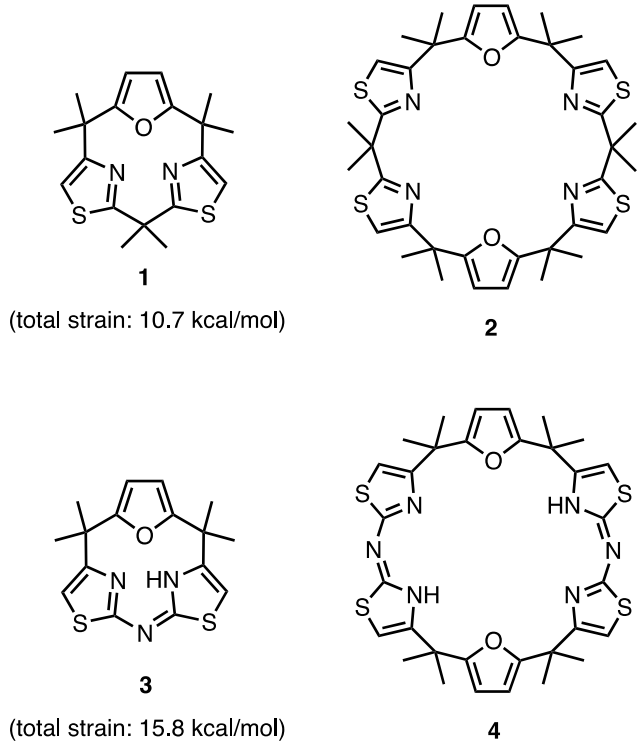


**Figure 1.** Thiazole-containing calix[3]- and calix[6]-type macrocycles.

Recently, we discovered that strain-based design of calix[3]-type macrocycles enables the direct macrocyclization of calix[1]furan[2]thiazole analogues via Hantzsch thiazole formation reaction between bis(α-bromoketone) and bis(thioamide) [9]. The macrocyclic ring strain in the calix[1]furan[2]thiazole system was susceptible to the chemical structure of the *meso*-bridge between two thiazole rings, and empirical estimation of the total strain based on steric repulsion was no longer reliable. Instead, calculation of the total strain using the StrainViz program [10] for the AFIR[11]-optimized conformations showed the feasibility of direct Hantzsch-type macrocyclization of calix[1]furan[2]thiazoles. In our previous study, we elucidated that *meso*-dimethylmethylene-bridged analogue **1** with total strain of 10.7 kcal/mol was obtained in 60% yield along with a ring-expanded analogue, calix[2]furan[4]thiazole **2**, in 16% yield (Figure 1). Whereas, *meso*-*N*($sp^2$)-bridged analogue **3** was

obtained only in 2% yield, and larger macrocycle **4** was the major product (32% yield). These experimental facts implied that the ring-size selectivity between ring-contracted and -expanded calix-type macrocycles would be switchable by total strain and substrate concentration. Here, we report the strain-based design and direct macrocyclization synthesis of novel calix[*n*]furan[2*n*]thiazoles (**5** (*n* = 1) and **6** (*n* = 2)) bearing *meso*-$CH_2$ bridges between thiazole units. The ring-size selectivity was clearly switched in the substrate concentration range between 2.5 mM and 25 mM. Unlike typical porphyrinogens, partially *meso*-$CH_2$-bridged calix[*n*]furan[2*n*]thiazoles **5** and **6** did not undergo air-oxidation in solution and in the solid state. Thus, **5** was successfully converted to corresponding calix[1]pyrrole[2]thiazole **9** through hydrolytic ring-opening reaction at the furan unit. Detailed strain analysis of novel calix[3]pyrrole analogues **5** and **9** provided insight into the correlation between strain energy and deformation angle or synthetic yield.

## EXPERIMENTAL

### Materials and Reagents

All of the solvents for optical measurements were purchased from WAKO Pure Chemical Industries Ltd., TCI Co., Ltd., Kanto Chemical Co., Inc., or Sigma-Aldrich Co., and used without further purification unless otherwise mentioned. Precursors **7** and **8** were prepared according to the reported procedures [12, 13].

### Instrumentation

All $^1$H and $^{13}$C NMR spectra were recorded using JEOL JMN-ECS400 spectrometer and chemical shifts were reported in parts per million (ppm) relative to an internal standard tetramethylsilane (δ = 0.00 ppm for $^1$H NMR in $CDCl_3$) or a solvent residual peak (δ = 77.16 ppm for $^{13}$C NMR in $CDCl_3$). Infrared spectra were measured using a JASCO Co. FT/IR-4600. High resolution electrospray ionization time-of-flight (HR-ESI-TOF) mass spectra were recorded on a Thermo Scientific Executive spectrometer. Matrix assisted laser desorption ionization time-of-flight (MALDI-TOF) mass spectra were recorded on a Bruker autoflex® maX spectrometer. Thin layer chromatography (TLC) was performed on a silica gel sheet, MERCK silica gel 60 F254. Preparative scale separations were performed by means of gravity column chromatography over silica gel (Wakosil® 60. 64 ~ 210 μm), and a recycling HPLC LaboACE LC-5060 equipped with two JAIGEL-2HR columns. Analytical high performance liquid chromatography using gel permeation column (GPC–HPLC) chromatograms were recorded using a JASCO MD-2018 photodiode array detector quipped with a JASCO PU-2089 pump, JASCO AS-2059 sampler, JASCO CO-2060 column thermostat. Single crystal X-ray diffraction data were collected with Rigaku XtaLAB P200 diffractometer equipped with a HyPix-6000HE detector using multi-layer mirror (Mo$K_a$ radiation = 0.71073 Å). All structures were solved using a dual-space algorithm (SHELXT) [14] and refined using full-matrix least-squares method (SHELXL) [15].

### Theoretical calculations

Geometry optimization and vibration analysis of **5** and **9** were performed by the global reaction route mapping (GRRM) program [16]. The density functional theory (DFT) calculations were carried out at the M06-2X[17]/6-311+G(2d,p) level of theory implemented in the Gaussian 16 program [18]. The initial structures were constructed from the three possible conformers determined by the systematic conformation search calculation of **1** in our previous work [9]. The vibrational

frequencies were computed to confirm whether the optimized geometry corresponded to stationary or saddle points on potential energy surface. The lowest energy conformer was determined by the comparison of Gibbs energy of the three conformers under standard condition. Additionally, the modeling of *meso*-C($sp^2$)H tautomers of **5** and **9** was derived from the *meso*-C($sp^3$)$H_2$ form. To confirm functional dependency for the stability of conformers and tautomers, the obtained structures were reoptimized at the B3LYP+D3[19,20]/6-311+G(2d,p) level of theory.

Strains of **5** and **9** were computed by the StrainViz analysis [10] at the M06-2X/6-311+G(2d,p) level of theory implemented in the Gaussian 16 program. The DFT structure of the lowest energy conformer was divided into three fragments with the same manner as our previous work [9] to evaluate four types of strain (total, bond, angle, and dihedral). The strain representation was visualized by the visual molecular dynamics software [21].

## RESULTS AND DISCUSSION

For the experimental analysis of ring-size selectivity, we searched for a suitable molecular motif of calix[3]-type macrocycle that has a moderate total strain between those of **1** and **3**. Generally, calix[3]-type products are entropically preferable to calix[6]-type products in the macrocyclization approach using monomeric components. However, when the calix[3]-type product has a larger total strain than that of the calix[6]-type analogue, the cyclization pathway for the calix[3]-type product is decelerated, thereby increasing in the selectivity of the calix[6]-type product.

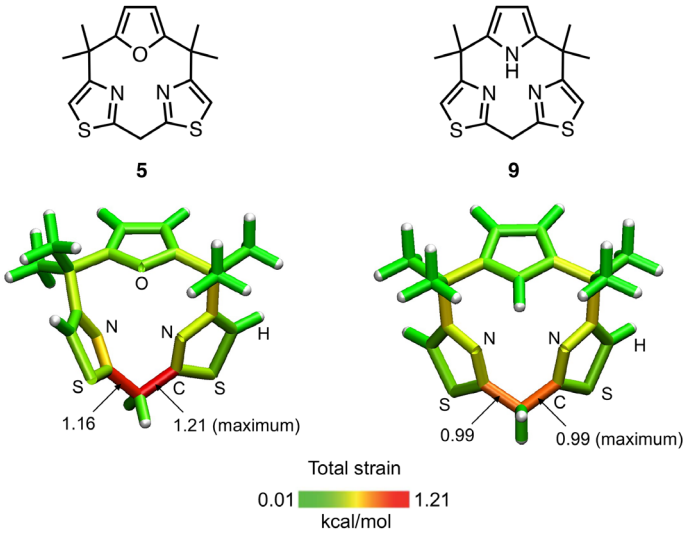


| Strain energy (kcal/mol) | **5** | **9** |
|---|---|---|
| Total strain | 11.2 | 10.6 |
| Bond strain | 0.5 | 0.5 |
| Angle strain | 1.7 | 2.2 |
| Dihedral strain | 9.0 | 7.9 |

**Figure 2.** (top) Visualization of the total ring strain for the optimized lowest energy conformations of **5** (left) and **9** (right) using the StrainViz analysis, and (bottom) calculated total, bond, angle, and dihedral strains.

When the *meso*-dimethylmethylene unit between two thiazole moieties in calix[1]furan[2]thiazole **1** was changed to a methylene, resulting **5** had a total strain of 11.2 kcal/mol as a result of a slight increase in the angle strain as compared to **1** (Figure 2). The relative stability of possible conformer/tautomer of **5** is summarized in Figure S3a in the Supporting Information. The energy minimized structure of **5** shows a partial cone conformation with two thiazole rings facing in different directions. Although *meso*-*N*-bridged analogue **3** adopted a gable-like conformation as a result of imine-enamine tautomerization to extend the π-conjugation over the two thiazole moieties, *meso*-C($sp^2$)H tautomer of **5** is found to be 3.8 kcal/mol more unstable than the *meso*-C($sp^3$)$H_2$ form. The StrainViz analysis indicates that the maximum strain is found for the C(thiazole)–$CH_2$(*meso*) bond as well as for **1**. The total strain of **5** is still smaller than that of **3** (15.8 kcal/mol) and calix[3]pyrrole (13.4 kcal/mol) [9], suggesting the feasibility of direct macrocyclization synthesis of **5** via Hantzsch reaction between corresponding bis(α-bromoketone) **7** and bis(thioamide) **8**. When the furan unit in **5** was changed to pyrrole, the total strain of calix[1]pyrrole[2]thiazole (**9**) was reduced to 10.6 kcal/mol due to the remarkable decrease in dihedral strain [10] (by 1.1 kcal/mol) arising from bond torsion. The most stable conformation of **9** is shown as a cone conformation (Figure S3b). The *meso*- C($sp^3$)$H_2$ form of **9** is also more stable than the C($sp^2$)H form. Thus, steric effects around the *meso*-$CH_2$ unit only give small perturbation for the total strains of macrocycles, compared to the *meso*-C($CH_3$)$_2$ unit. Considering the results of StrainViz analysis, we decided to investigate the direct macrocyclization synthesis of **5** under various concentrations to switch size-selectivity.

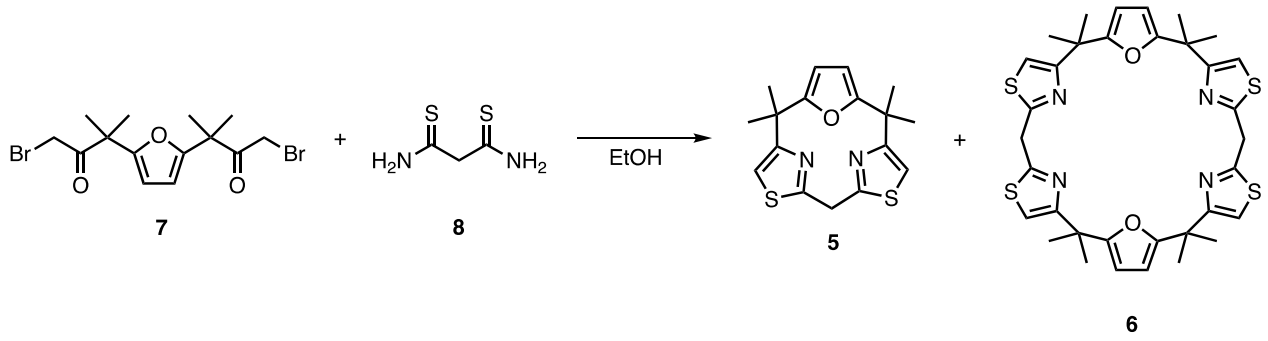


| substrate concentration (mmol/L) | yield of **5** (%) | yield of **6** (%) |
|---|---|---|
| 0.50 | 42 | 1 |
| 1.0 | 48 | 7 |
| 2.5 | 40 | 12 |
| 5.0 | 27 | 20 |
| 10 | 14 | 24 |
| 25 | 8 | 25 |
| 50 | 3 | 20 |
| 100 | 2 | 17 |

**Scheme 1.** Synthesis of calix[*n*]furan[2*n*]thiazoles **5** and **6** under various substrate concentrations. Yields were determined by NMR spectroscopy using triphenylmethane as a standard.

Condensation reaction between α-bromoketone **7** and an equimolar amount of thioamide **8** in ethanol at a 2.5 mM concentration under the conditions reported for the synthesis of **1** and **2** gave the calix[3]-type product **5** was formed in 40% yield along with the calix[6]-type macrocycle **6** in 12% yield (Scheme 1). The decrease in the yield of **5** and the slight increase in the selectivity of **6** compared to the reaction for **1** and **2** were attributable to the larger total strain of **5** than that of **1**. When similar reactions were conducted under diluted conditions at 1.0 and 0.50 mM, the formation of **6** was effectively suppressed with a concomitant increase in the yield of **5** to 48 and 42%, respectively. In contrast, the yield of **5** gradually decreased with increasing substrate concentration. The yield of **6** increased from 12% (at 2.5 mM) to 25% (at 25 mM), although further increase in the concentration resulted in the decreased yields for both **5** and **6**. The GPC–HPLC and mass spectrometric analyses of the reaction mixture exhibited the formation of a significant amount of larger analogues, such as calix[9]- and calix[12]-type macrocycles, at 25 mM concentration without specific selectivity (Figure S6 and S7). Under the optimized conditions, calix[3]- and calix[6]-type macrocycles were isolated in 30% and 17% yields at the concentrations of 1.0 and 25 mM, respectively.

Calix[1]furan[2]thiazole **5** showed a singlet signal at 4.50 ppm for *meso*-methylene protons in the $^1$H-NMR spectrum recorded in $CDCl_3$ (Figure S8). The observed proton signal pattern indicated the time-averaged $C_{2v}$ molecular symmetry as observed for **1**. The *meso*-C($sp^2$)H-bridged tautomer, which could be generated through imine–enamine-like tautomerization, was not observed in the $^1$H-NMR spectrum. Calix[6]-type macrocycle **6** also exhibited a singlet signal at 4.57 ppm which is assignable to the *meso*-$CH_2$ protons (Figure S10). High-resolution ESI-TOF mass spectrometry revealed the cation and anion peaks for **5** and **6** at *m*/*z* = 331.0921 and 659.1660 which were assigned to [**5** + H]$^+$ (calculated for $C_{17}H_{19}ON_2S_2$, *m*/*z* = 331.0933) and [**6** – H]$^-$ (calculated for $C_{34}H_{36}O_2N_4S_4$, *m*/*z* = 659.1648), respectively. Although calix[*n*]pyrroles with *meso*-C($sp^3$)H units are readily oxidized under aerobic conditions, no air-oxidation of macrocycles **5** and **6** was observed in solution and in the solid state. This can be explained by the electron-deficient nature of thiazole rings as compared to pyrrole. Upon treatment with hydrochloric acid and ethanol, compound **5** underwent hydrolysis of the furan ring to form a 1,4-diketone moiety **10** in 45% yield. Further Paal–Knorr reaction of **10** with ammonium acetate afforded calix[1]pyrrole[2]thiazole **9** bearing a *meso*-$CH_2$ bridge in 74% yield (Figure 3a).

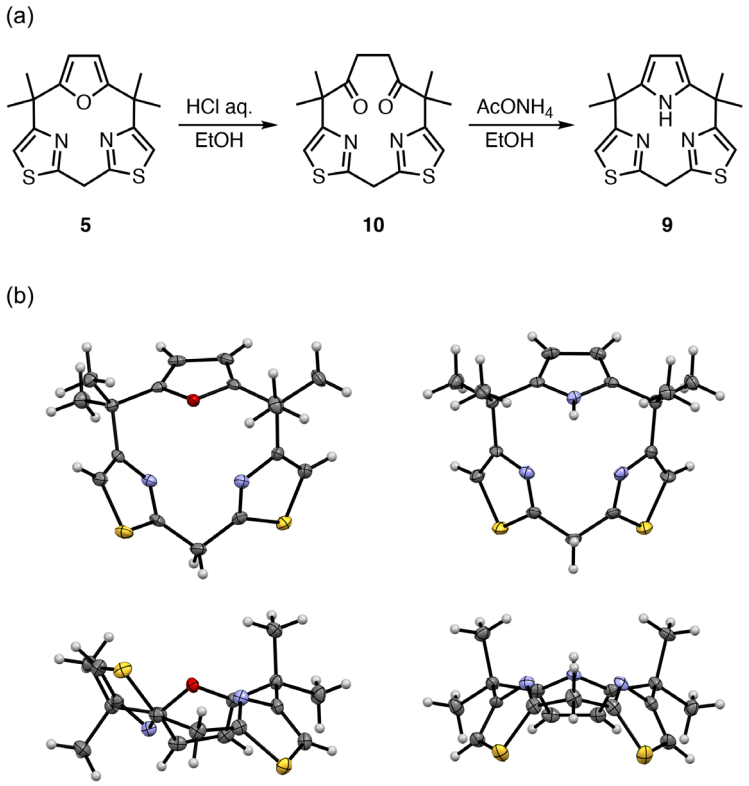


**Figure 3.** (a) Synthesis of calix[1]pyrrole[2]thiazole **9**. (b) Single crystal X-ray structures of (left) **5** and (right) **9** with thermal ellipsoids drawn at the 50% probability level. (H, white; C, gray; N, blue; O, red; and S, yellow).

Single crystals of **5** suitable for X-ray diffraction analysis were grown by vapor diffusion of *n*-hexane into an ethyl acetate solution of **5**. In the crystalline state, **5** adopted a partial cone conformation, as predicted by the theoretical calculations (Figure 3b). The bond lengths for C(thiazole)–$CH_2$(*meso*) were 1.511 and 1.512 Å, and the bond angle of C(thiazole)–C(*meso*)– C(thiazole) was 107.37°, indicating the $sp^3$-hybridization for the *meso*-carbon atom between thiazole rings. Pyrrole analogue **9** showed a cone conformation in which the N(pyrrole)–N(thiazole) distance was observed in the range of 2.70–2.72 Å, while the N(thiazole)–N(thiazole) distance was 2.86 Å. The C(thiazole)–$CH_2$(*meso*) of 1.50–1.52 Å also indicated the existence of the *meso*-C($sp^3$)$H_2$ bridge.

The crystal structures of **5** and **9** allowed deformation angle [22] analysis around the furan and pyrrole units. Deformation angle $\alpha$ shows deformation of pyrrole or furan rings from planarity, while deformation angle $\beta$ represents displacement of the *meso*-carbon atom from the bow of the heteroaromatic ring. Table 1 summarizes the deformation angles and calculated total strains of calix[3]pyrrole and its thiazole-containing analogues. The furan-containing analogues **1**, **3**, and **5** exhibited a trend that the deformation angles $\alpha$ and $\beta$ increase with increasing total strain. A similar tendency was also observed for the pyrrole derivative **9** compared to calix[3]pyrrole. These results confirmed that the accuracy of the StrainViz-based evaluation for calix[3]-type macrocycles for predicting ring strain as well as favorable conformations.

**Table 1.** Deformation angle[a] $\alpha$ and $\beta$ of furan or pyrrole units embedded in calix[3]-type macrocycles.

| Compound | 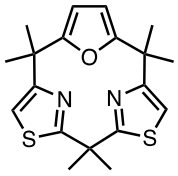 **1** | 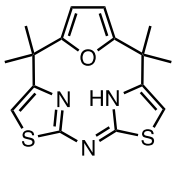 **3** | 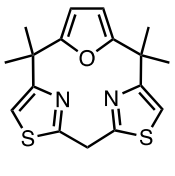 **5** | 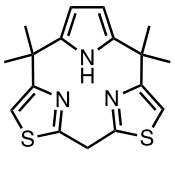 **9** | 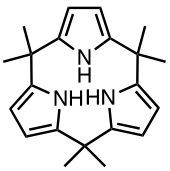 calix[3]pyrrole |
|---|---|---|---|---|---|
| Deformation angle α (°) | 2.05[b] | 2.58 | 2.26 | 2.41 | 2.52[c] |
| Deformation angle β (°) | 6.42[b] | 8.96 | 6.65 | 5.59 | 9.20[c] |
| Total strain (kcal/mol) | 10.7[d] | 15.8[c] | 11.2 | 10.6 | 13.4[d] |

[a] Deformation angles $\alpha$ and $\beta$ for pyrrole or furan are defined by the averaged deviation angles between the mean planes of X－C(3)－C(4) and X－C(2)－C(3), and the mean plane X－C(2)－C(3) and a C(2)－C(meso) bond, respectively. (X = N or O).
[b] Optimized structure data from ref. 9
[c] The averaged angles of three pyrrole units from ref. 5
[d] Data from ref. 9

## CONCLUSION

In conclusion, novel calixpyrrole analogues **5** and **6** bearing methylene-bridged dithiazole units have been synthesized via Hantzsch-type direct macrocyclization. The ring-size selectivity was significantly altered depending on the substrate concentration; calix[3]-type **5** was formed almost exclusively at 0.50 mM, while **6** was the major product above 10 mM. These reactions have provided a rare example of size-selectivity switching between contracted and expanded calix-type macrocycles. The *meso*-$CH_2$ bridge between two thiazole rings in **5** and **6** was stable enough to resist air-oxidation. Therefore, calix[1]furan[2]thiazole **5** was successfully converted to calix[1]pyrrole[2]thiazole via the furan ring hydrolysis followed by the Paal–Knorr pyrrole formation reaction. The deformation angle analysis of novel calix[3]pyrrole analogues **5** and **9** using single crystal X-ray structures demonstrated that StrainViz analysis is useful for predicting solid state conformations and quantitative evaluation of macrocyclic ring strain. The strain-based design and reliable synthesis of thiazole-containing calixpyrrole analogues would contribute to expand the coordination and anion binding chemistry.

**Acknowledgements**

This work was partly supported by a JSPS Grant-in-Aid for Challenging Research (Exploratory) (No. 24K2178704), Scientific Research (B) (No. 22H0205802), and JST FOREST Program (No. PJ2522A005), the Asahi Glass Foundation of

which Y. Inokuma is the principal investigator. The Institute for Chemical Reaction Design and Discovery (ICReDD) was established by World Premier International Research Initiative (WPI), MEXT, Japan.

## REFERENCES


1. a) Escobar L, Sun Q, Ballester P. *Acc. Chem. Res.* 2023; **56**: 500–513; b) Gale PA, Anzenbacher P, Sessler JL. *Coord. Chem. Rev.* 2001; **222**: 57–102. c) Gale PA, Sessler JL, Král V. *Chem. Commun.* 1999; 1–8.
2. Ruppert H, Sigmund LM, Greb L. *Chem. Commun.* 2021; **57**: 11751–11763.
3. a) Kim DS, Sessler JL. *Chem. Soc. Rev.* 2015; **44**: 532–546; b) Mamardashvili GM, Mamardashvili NZ, Koifman OI. *Russ. Chem. Rev.* 2015; **84**: 279–287; c) Saha I, Lee JT, Lee C-H. *Eur. J. Org. Chem.* 2015; **2015**: 3859–3885.
4. Sessler JL, Anzenbacher Jr. P, Shriver JA, Jursíková K, Lynch VM, Marquez M. *J. Am. Chem. Soc*. 2000; **122**: 12061–12062.
5. Inaba Y, Nomata Y, Ide Y, Pirillo J, Hijikata Y, Yoneda T, Osuka A, Sessler JL, Inokuma Y. *J. Am. Chem. Soc*. 2021; **143**: 12355–12360.
6. a) Cafeo G, Kohnke FH, La Torre GL, White AJP, Williams DJ. *Chem. Commun.* 2000; 1207–1208; b) Cafeo G, Gattuso G, Kohnke FH, Notti A, Occhipinti S, Pappalardo S, Parisi MF. *Angew. Chem. Int. Ed.* 2002; **41**: 2122–2126.
7. a) Kozhushkov S, Haumann T, Boese R, Knieriem B, Scheib S, Bauerle P, Meijere A de. *Angew. Chem. Int. Ed. Engl.* 1995; **34**: 781–783; b) Lee G-A, Wang W-C, Shieh M, Kuo T-S. *Chem. Commun.* 2010; **46**: 5009–5011; c) Lee G-A, Shih Y-F, Lin H-C, Wang W-C, Chan H-T, Lee H-Y, Lee C-Y. *ChemistrySelect* 2020; **5**: 8518–8521; d) Chun Y, Singh NJ, Hwang I-C, Lee JW, Yu SU, Kim KS. *Nat. Commun.* 2013; **4**: 1797; e) Král V, Gale PA, Anzenbacher Jr. P, Jursíková K, Lynch VM, Sessler JL. *Chem. Commun.* 1998; 9–10.
8. a) Inaba Y, Yang J, Kakibayashi Y, Yoneda T, Ide Y, Hijikata Y, Pirillo J, Saha R, Sessler JL, Inokuma Y. *Angew. Chem. Int. Ed.* 2023; **62**: e202301460; b) Namor AFD de, Abbas I. *J. Phys. Chem. B* 2007; **111**: 5803–5810; c) Chellappan K, Singh NJ, Hwang I-C, Lee JW, Kim KS. *Angew. Chem. Int. Ed.* 2005; **44**: 2899–2903; d) Black DS, Craig DC, Kumar N. *Tetrahedron Lett.* 1995; **36**: 8075–8078; e) Poulsen T, Nielsen KA, Bond AD, Jeppesen JO. *Org. Lett.* 2007; **9**: 5485–5488.
9. Watanabe K, Shibata K, Ichino T, Ide Y, Yoneda T, Maeda S, Inokuma Y. *Inorg. Chem. Front.* 2024; **11**: 3548–3554.
10. Colwell CE, Price TW, Stauch T, Jasti R. *Chem. Sci.* 2020; **11**: 3923–3930.
11. Maeda S, Taketsugu T, Morokuma K. *J. Comput. Chem.* 2014; **35**: 166–173.
12. Fujita H, Arai S, Arakawa H, Hamamoto K, Kato T, Arai T, Hotta K, Hosokawa N, Ohbayashi T, Takahashi C, Inokuma Y, Tamai I, Yano S, Kunishima M, Watanabe Y. *Bioorg. Med. Chem.* 2024; **102**: 11674–11684.
13. Bret J-M, Castan P, Laurent J-P. *J. Chem. Soc. Dalton Trans.* 1984; 1975–1980.
14. Sheldrick GM. *Acta Cryst.* 2015; **A71**: 3–8.
15. Sheldrick GM. *Acta Cryst.* 2015; **C71**: 3–8.
16. GRRM. https://global.hpc.co.jp/products/grrm23/ (accessed December 18, 2024)
17. Zhao Y, Truhlar DG. *Theor. Chem. Account* 2008; **120**: 215–241.
18. Frisch MJ, Trucks GW, Schlegel HB, Scuseria GE, Robb MA, Cheeseman JR, Scalmani G, Barone V, Petersson GA, Nakatsuji H, Li X, Caricato M, Marenich AV, Bloino J, Janesko BG, Gomperts R, Mennucci B, Hratchian HP, Ortiz JV, Izmaylov AF, Sonnenberg JL, Williams-Young D, Ding F, Lipparini F, Egidi F, Goings J, Peng B, Petrone A, Henderson

T, Ranasinghe D, Zakrzewski VG., Gao J, Rega N, Zheng G, Liang W, Hada M, Ehara M, Toyota K, Fukuda R, Hasegawa J, Ishida M, Nakajima T, Honda Y, Kitao O, Nakai H, Vreven T, Throssell K, Montgomery Jr. JA, Peralta JE, Ogliaro F, Bearpark MJ, Heyd JJ, Brothers EN, Kudin KN, Staroverov VN, Keith TA, Kobayashi R, Normand J, Raghavachari K, Rendell AP, Burant JC, Iyengar SS, Tomasi J, Cossi M, Millam JM, Klene M, Adamo C, Cammi R, Ochterski JW, Martin RL, Morokuma K, Farkas O, Foresman JB, Fox DJ, Gaussian 16, Revision C.01; Gaussian, Inc., Wallingford CT, 2019.

19. a) Becke AD. *Phys. Rev. A* 1988; **38**: 3098–3100; b) Becke AD. *J. Phys. Chem*. 1993; **98**: 5648–5652; c) Lee C, Yang W, Parr RG. *Phys. Rev. B* 1988; **37**: 785–789.
20. Grimme S, Antony J, Ehrlich S, Krieg HA. *J. Chem. Phys.* 2010; **132**: 154104.
21. Visual Molecular Dynamics. https://www.ks.uiuc.edu/Research/vmd/. (accessed December 18, 2024)
22. Tobe Y, Ueda K, Kakiuchi K, Odaira Y, Kai Y, Kasai N. *Tetrahedron* 1986; **42**: 1851–1858.

# Size-selective synthesis of calix[*n*]furan[2*n*]thiazoles bearing *meso*-$CH_2$ bridges

Kotaro Shibata, Takuma Nakabayashi, Keita Watanabe, Yuki Ide, Tomoya Ichino, and Yasuhide Inokuma

Thiazole-containing calix[3]- and calix[6]pyrrole-type macrocycles bearing *meso*-$CH_2$ bridges were synthesized via Hantzsch thiazole formation reaction. The product size selectivity was significantly changed depending on substrate concentration. Calix[1]furan[2]thiazole was further converted to calix[1]pyrrole[2]thiazole. StrainViz analysis of novel macrocycles predicted the conformations and the magnitude of ring strain, which was also confirmed experimentally by deformation angle analysis.